Control Strategy of Flyback Microinverter with Hybrid Mode for PV AC Modules

Sung-Ho Lee, Woo-Jun Cha, Jung-Min Kwon, *Member*, *IEEE* and Bong-Hwan Kwon, *Member*, *IEEE*

***Abstract*— This paper presents a control strategy of a flyback microinverter with hybrid operation mode for photovoltaic (PV) AC modules. The proposed control strategy consists of two com-ponents: the proportional-resonant (PR) controller with the harmonic compensator (HC), and the hybrid nominal duty ratio. Compared to the conventional control strategy using the propor-tional-integral (PI) controller, the PR controller with HC provides higher system gain at the fundamental and harmonic frequencies of the grid without using high proportional gain in both operation modes. Then, it enhances tracking speed and disturbance rejec-tion performances satisfying the desired stability. Moreover, by applying the hybrid nominal duty ratio yielded from the proposed operation mode selection, the disturbance rejection is achieved more effectively, and the control burden is reduced. Finally, the simulation and experiment results were shown to verify the tracking speed and disturbance rejection performances of the proposed control strategy.**

***Index Terms*— Right-half-plane zero, current control scheme, single-stage inverter, PV module.**

I. INTRODUCTION

With an increase of attention in renewable energy sources, the PV energy has been widely utilized in various industrial fields. The PV power systems can be classified into centralized, string, and ac module systems [1]. Among them, in the ac module system, a low-power grid-connected inverter called as the microinverter is mounted on a single PV module; it can track the individual maximum power point (MPP), and so reduces power losses by PV module mismatch and partial shading [2]-[4]. Moreover, the ac module system has higher reliability and easier maintenance than those of other PV systems [5]. Thus, with these advantages, the ac module PV system has been recently considered as a trend of the future PV power systems.

The worth of the microinverter is evaluated by its power conversion efficiency, the shape of output current, power density, reliability, and cost [6]-[8]. To meet these requirements, a single-stage flyback inverter topology has been adopted due to its simple circuit structure and potential for high efficiency and reliability. Moreover, the flyback inverter topology has both step-down and step-up functions; this characteristic is suitable for the PV applications where the inverter should operate in wide voltage range.

When the flyback inverter operates under the constant switching frequency, the operation modes can be classified as the discontinuous current mode (DCM) [9]-[14] and continuous current mode (CCM) [15]-[17]. Actually, the PV inverter called as the CCM flyback inverter has both operation modes; it inevitably operates in DCM at the low instantaneous power level or low solar irradiation level although it operates in CCM at all instantaneous power levels for rated average power. Then, it can be regarded that the flyback inverter has hybrid operation mode over whole ac-line period. Compared to a flyback inverter only with DCM, the flyback inverter with hybrid mode has the numerous merits such as higher efficiency with lower current stress, higher power capability, and easier filter design. However, the control input-to-output current transfer function of the flyback inverter in the CCM region has a right half-plane (RHP) zero which results in the limitations of increasing the system gain and controller bandwidth. Since the operating point varies widely in the PV inverter applications, especially, the controller should cover the minimum RHP zero. When a conventional PI controller is applied to the flyback inverter with hybrid mode, the proportional gain is designed to be relatively low for ensuring stability in all operating points [17].

The system gain of the flyback inverter in the DCM region is inherently much low. To achieve fast reference tracking and disturbance rejection performances, the high gain feed-back controller is required in the DCM operation. However, when the conventional PI controller is applied, the control gain is limited by the RHP zero in CCM. As a result, it causes unacceptable power quality and high total harmonic distortion (THD) by the poor control performance in DCM [15]. This is the reason why the use of the flyback inverter with hybrid mode is limited despite its many advantages.

To avoid the mentioned problem, some previous studies in [15], [16] control the primary current instead of controlling the output current because there is no RHP zero in the transfer function for the control input to the primary current. The control approach bypasses the difficulties posed by the RHP zero. However, the power quality is low because this approach controls the output current indirectly.

The PR controller is an alternative of the PI controller. It provides an infinite gain at a selected resonant frequency without using high proportional gain [18]-[20]. Moreover, because the controller has flexibility of selecting the resonant

Manuscript received March 29, 2015; revised June 24, 2015 and July 31, 2015; accepted September 1, 2015.

S.-H. Lee, W.-J. Cha, and B.-H. Kwon are with the Department of Electronic and Electrical Engineering, Pohang University of Science and Technology, Pohang, Gyungbuk 790-784, Korea (e-mail: mulem@postech.ac.kr; woojun79@postech.ac.kr; bhkwon@postech.ac.kr).

J.-M. Kwon is with the Department of Electrical Engineering, Hanbat University, Daejeon 305-719, Korea (e-mail: jmkwon@hanbat.ac.kr).

This article has been accepted for publication in a future issue of this journal, but has not been fully edited. Content may change prior to final publication. Citation information: DOI 10.1109/TIE.2015.2481365, IEEE Transactions on Industrial Electronics

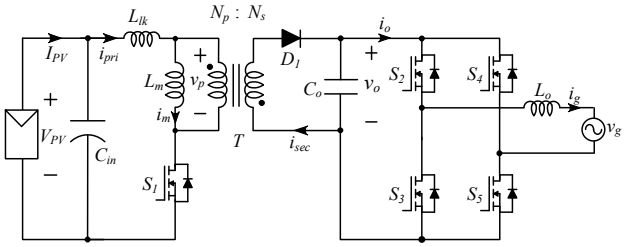

Fig. 1. Circuit diagram of the flyback microinverter.

frequency, adding multiple PR controllers such as the harmonic compensator is possible for compensating the harmonics of the selected fundamental frequency.

In this paper, the current control strategy of the flyback microinverter with hybrid mode is proposed. The proposed control strategy consists of two components: the PR controller with HC and the hybrid nominal duty ratio. The PR controller with HC provides high gain at the fundamental and harmonic frequencies of the grid and achieves the zero-tracking error in both operation modes. The hybrid nominal duty ratio performs as a feedforward control input and is determined by the proposed operation mode selection. By applying the hybrid nominal duty ratio according to proper operation region, it can achieve more effective disturbance rejection and faster dynamics. Thus, the proposed control strategy gives the higher tracking performance and better disturbance rejection in both operation modes and strengthens the many advantages of the flyback inverter with hybrid mode. In Section II, the basic operation of the flyback inverter for each mode is introduced. Section III represents the system dynamic characteristic according to each operation mode, and handles with the problems on the conventional current control with the PI controller. Then, the proposed control strategy is introduced, and its superiority and validity are represented from theoretical analysis. Finally, the simulation and experimental results are shown in Section IV.

II. Principle Operation of the Flyback Inverter with Hybrid Mode

Fig.1 shows a circuit diagram of the flyback microinverter; it consists of an input capacitor C_{in}, a flyback converter with turn ratio n (N_s / N_p), a full-bridge type unfolding circuit (S_2 − S_5), and an output filter. The flyback converter operates under the high switching frequency to convert PV power into rectified sinusoidal waveform. The unfolding circuit works under the grid frequency f to inject sinusoidal ac current into the grid; switches S_2 and S_5 are turned on during the positive half-cycle of the grid voltage v_g, while S_3 and S_4 are turned on during the negative half-cycle.

A. Steady-state analysis of DCM and CCM operations

Under the constant switching frequency f_s, the operation modes are classified into DCM and CCM. In DCM, the magnetizing current i_m becomes zero within each switching period T_s, and the transformer T is completely demagnetized as shown in Fig. 2. When S_1 is turned on, the primary current i_{pri} is stored

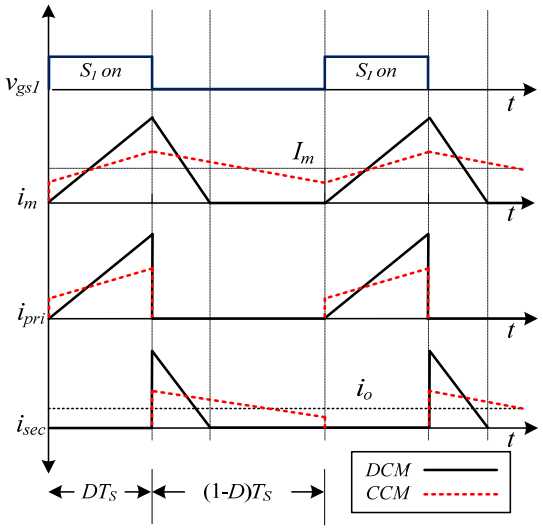

Fig. 2. Key waveforms in DCM and CCM.

in the magnetizing inductance L_m, and its peak value is expressed as follows:

$$I_{pri,pk\_DCM}(t) = \frac{V_{PV}}{L_m} D_{DCM}(t) T_s \tag{1}$$

where D_{DCM} is the duty ratio in DCM. The energy E_{Lm} stored in L_m is expressed as

$$E_{Lm} = \frac{1}{2} L_m I_{pri,pk}{}^2(t) = \frac{(V_{PV} D_{DCM}(t) T_s)^2}{2L_m}. \tag{2}$$

Assuming lossless operation in the inverter, the power balance equations can be obtained as

$$V_{PV} I_{PV} = \frac{V_g I_g}{2} = P_o \tag{3}$$

$$V_{PV} I_{pri}(t) = v_g(t) i_g(t) = V_g I_g \sin^2 \omega t \tag{4}$$

where V_{PV} and I_{PV} are the average values of the voltage and current for a PV module. v_g and i_g are the grid voltage and grid current; V_g and I_g are the peak values of v_g and i_g, respectively. P_o is the average output power. I_{pri} is the average primary current. ω is the angular frequency of the grid voltage. If there is no loss, the energy stored in L_m is equal to the energy transferred to the grid. Assuming $|v_g| \approx v_o$, from (2)-(4), D_{DCM} can be derived as

$$\begin{aligned} D_{DCM}(t) &= \frac{2}{V_{PV}} \sqrt{P_o L_m f_s} \left|\sin \omega t\right| \\ &= d_{DCM,pk} \left|\sin \omega t\right| \end{aligned} \tag{5}$$

where $d_{DCM,pk}$ is the peak value of D_{DCM}. In CCM, L_m is applied to V_{PV} during the turn-on time of S_1, while the voltage across L_m is reflected the output voltage during the turn-off time. Using the voltage-seconds law for L_m, the duty ratio D_{CCM} in CCM is

This article has been accepted for publication in a future issue of this journal, but has not been fully edited. Content may change prior to final publication. Citation information: DOI 10.1109/TIE.2015.2481365, IEEE Transactions on Industrial Electronics

calculated as

$$D_{CCM}(t)=\frac{V_g\left|\sin\omega t\right|}{nV_{PV}+V_g\left|\sin\omega t\right|}. \tag{6}$$

The duties D_{DCM} and D_{CCM} determine the relationship between the input voltage V_{PV} and output voltage v_o.

As mentioned above, the peak value of the primary current in DCM is expressed as the equation (1). In case of CCM, as shown in Fig. 2, the peak value of the primary current $I_{pri,\,pk\_CCM}$ is equal to the sum of the average magnetizing current I_m and the ripple component. Because the magnetizing current is the same as the primary current when S_1 is turned on, its average value can be expressed using the average value of the primary current I_{pri} and the duty ratio D_{CCM} as

$$I_m(t)=\frac{I_{pri}(t)}{D_{CCM}(t)}. \tag{7}$$

Thus, from Fig. 2 and the power relationship in (2), the peak value of the primary current $I_{pri,\,pk\_CCM}$ is calculated as

$$\begin{aligned} I_{pri,pk\_CCM}(t)&=\frac{I_{pri}(t)}{D_{CCM}(t)}+\frac{V_{PV}D_{CCM}(t)T_S}{2L_m}\\ &=\frac{i_o}{V_{PV}}(nV_{PV}+\left|v_g(t)\right|)+\frac{1}{2L_mf_s}V_{PV}\frac{\left|v_g(t)\right|}{nV_{PV}+\left|v_g(t)\right|}. \end{aligned} \tag{8}$$

The peak value of the secondary current is the same as the peak value of i_{pri} for each mode divided by the turn ratio n.

B. Flyback microinverter with hybrid mode

Under the DCM operation, the turn-off time t_{off} is divided into the falling time t_f and the zero time Δt. The time t_f is constant and is given by [6]

$$t_f=\frac{nV_{PV}d_{DCM,pk}}{V_g}T_s=n\lambda d_{DCM,pk}T_s \tag{9}$$

where V_{PV}/V_g is denoted as λ. Because i_m is zero before end of each switching period T_s, the following condition (10) is satisfied in DCM

$$t_{on}(t)+t_f=d_{DCM,pk}(\left|\sin\omega t\right|+n\lambda)T_s\le T_s. \tag{10}$$

With an increase of the output power, D_{DCM} also increases, and the sum of the turn-on time and falling time becomes T_s. Thus, from (5) and (10), the critical duty ratio D_{cri} can be obtained as follows:

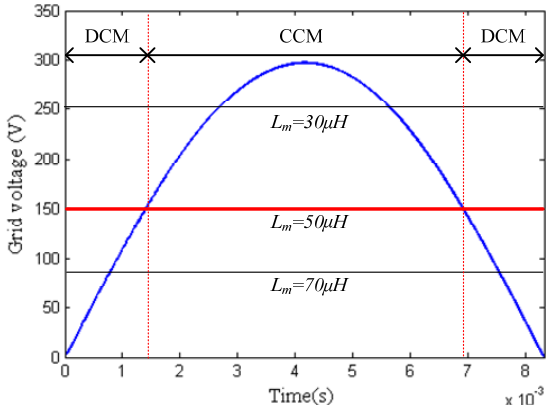

Fig. 3. Operation regions of the flyback inverter during a half-cycle of the grid voltage.

$$\begin{aligned} D_{cri}(t)&=\frac{t_{on}(t)}{T_s}=\frac{d_{DCM,pk}T_s\left|\sin\omega t\right|}{d_{DCM,pk}(\left|\sin\omega t\right|+n\lambda)T_s}\\ &=\frac{V_g\left|\sin\omega t\right|}{nV_{PV}+V_g\left|\sin\omega t\right|}. \end{aligned} \tag{11}$$

From (11), the fact that the duty ratio D_{DCM} is equal to D_{CCM} under boundary condition is verified, and the flyback operates in the DCM region when D_{DCM} is smaller than D_{CCM}. Fig. 3 shows the operation regions of the flyback inverter in a half-cycle of the grid under conditions given in Table I. As shown in Fig. 3, the flyback inverter operates in DCM at the low instantaneous power level or low solar irradiation level although it operates in CCM region above a certain power level in ac line period. Because the flyback inverter has both operation modes over whole ac line period, it performs as the flyback inverter with hybrid mode.

The boundary between DCM and CCM regions varies according to the magnetizing inductance L_m. Lower L_m results in larger DCM region at the given output power. The critical magnetizing inductance $L_{m,cri}$ is derived from (5) and (6) as follows:

$$L_{m,cri}=\frac{1}{4P_of_s}\left(\frac{V_{PV}V_g}{nV_{PV}+V_g}\right)^2. \tag{12}$$

To make the flyback inverter only operate in the DCM region, L_m should be lower than $L_{m,cri}$ at a certain output power. The flyback inverter only with the DCM region suffers from the high current stress which causes high power losses and limits the increase of the power capacity. As L_m increases, the CCM region increases, and the maximum current stress gradually decreases. Thus, the high L_m enhances the efficiency and power capacity. However, when setting the value of L_m, there is a trade-off between the efficiency and transformer size; higher L_m gives the lower current stress but a larger transformer size. Thus, the design of L_m for the flyback inverter with hybrid mode should be above $L_{m,cri}$, and consider the acceptable current stress and transformer size.

This article has been accepted for publication in a future issue of this journal, but has not been fully edited. Content may change prior to final publication. Citation information: DOI 10.1109/TIE.2015.2481365, IEEE Transactions on Industrial Electronics

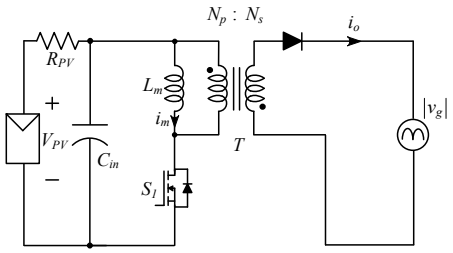

Fig. 4. Equivalent circuit of the grid-connected flyback microinverter.

III. Analysis for Control Strategy of Flyback Microinverter with Hybrid Mode

A. Control issues

In the flyback microinverter with hybrid mode, the current controller should ensure the reference tracking and disturbance rejection performances in both operation regions. Fig. 4 shows the equivalent circuit of the grid-connected flyback micro-inverter. Using the control input-to-output current transfer function introduced in [15], the transfer function G_{id_DCM} in DCM can be expressed as follows:

$$G_{id\_DCM} = \frac{V_{PV}}{V_{g,rms}}\sqrt{\frac{P_o}{2L_m f_s}} \tag{13}$$

where $V_{g,rms}$ is the rms value of the grid voltage. Eqn. (13) is noted that the system gain in DCM is constant and very low at all frequency ranges. Using a small signal modeling, the transfer function G_{id_CCM} in CCM can be represented as

$$G_{id\_CCM} = \frac{As+B}{R_{in}C_{in}L_m s^2 + L_m s + D_{CCM}{}^2 R_{PV}} - \frac{I_{Lm}}{n}$$

where

$$A = R_{PV}C_{in}\frac{(1-D_{CCM})(V_{Cin}+\frac{v_g}{n})}{n} \tag{14}$$

$$B = \frac{1-D_{CCM}}{n}(V_{Cin}+\frac{v_g}{n} - D_{CCM}I_{Lm}R_{PV}).$$

From (14), it is observed that the control input-to-output current transfer function in CCM has an RHP zero. The RHP zero varies according to the operating points, and its minimum value is at the peak of the grid voltage under maximum output power. Thus, the minimum RHP zero should be considered when the controller for the flyback inverter with hybrid mode is designed.

In the conventional control system [17], the PI controller is used to ensure the reference tracking and disturbance rejection performances. Fig. 5 shows open-loop Bode plots of the compensated systems by the conventional PI controller. Used parameters are listed in Table I. The operating point in DCM is at the instantaneous power 25W under the rated average output power. While, the point in the CCM is the peak of v_g under the rated average output power where it is the minimum RHP zero. The proportional gain k_p of the PI controller is tuned to be low to ensure the stability in the operation point with the minimum RHP zero. Thus, the gains of the conventional PI controller are set as follows: the proportional integral gain k_p = 0.08 and k_i = 64. As shown in Fig. 5, the system gain at the fundamental and its harmonic frequencies of the grid in DCM is much lower than that in CCM although the integral action of the PI controller gives high DC gain at the origin. This makes the flyback inverter in the DCM region be unable to ensure tracking the reference and rejecting disturbances by the PV and grid voltages effect. To increase the system gain at those frequencies, a high proportional gain is required. However, it raises the system gain at all frequencies and so could make the flyback inverter in the CCM region become unstable. Consequently, when applying the conventional PI controller to the flyback inverter with hybrid mode, there is a trade-off between control performance in DCM and stability in CCM.

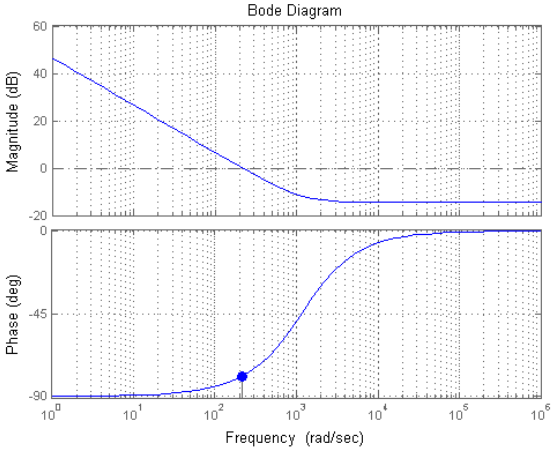

(a)

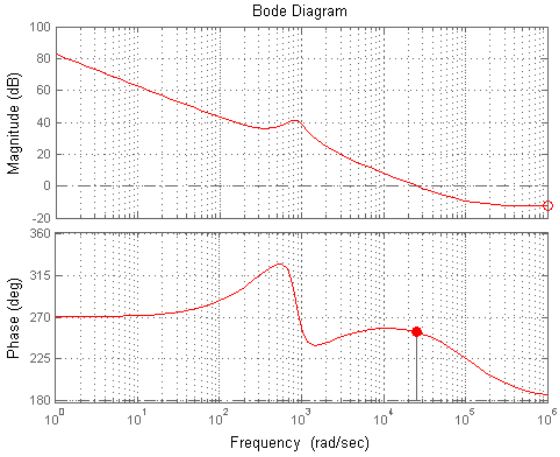

(b)

Fig. 5. Open-loop Bode plots of the compensated system by the conventional PI controller. (a) In DCM. (b) In CCM.

This article has been accepted for publication in a future issue of this journal, but has not been fully edited. Content may change prior to final publication. Citation information: DOI 10.1109/TIE.2015.2481365, IEEE Transactions on Industrial Electronics

B. *Proposed control strategy*

To satisfy the desired control performance and stability in both operation modes, the PR controller can be developed, and its transfer function is expressed as

$$C_{PR}(s) = k_p + \frac{k_r s}{s^2 + \omega^2} \tag{15}$$

where k_r is the resonant gain. The PR controller in (15) has an infinite gain at the grid frequency. However, the infinite gain would degrade the control performance and even cause the system to become unstable. In the practical implementation, the following form of the PR controller can be adopted as

$$C_{PR}(s) = k_p + \frac{2k_r\omega_c s}{s^2 + 2\omega_c s + \omega^2} \tag{16}$$

where ω_c is chosen to widen the controller bandwidth and determines the -3 dB cutoff frequency of the controller. That is, the magnitude of the compensator becomes $k_r/\sqrt{2}$ at ω-ω_c or ω+ω_c. In the PR controller, k_p is selected in the same way as that of a PI controller. That is, it is designed by the stability of the compensated systems considering the minimum RHP zero. The gain k_r is tuned relatively high to minimize steady-state error but it is limited by the stability. In case of the proposed PR controller, the gains k_r and ω_c are 20 and 16, respectively; k_r is selected to make the system have the phase margin above 45° to ensure the stability in practice. In addition, the harmonic compensator is able to alleviate errors for the selective harmonic frequencies, and its transfer function is represented as

$$C_{HC}(s) = \sum_{h=3,5,7\ldots} \frac{2k_{rh}\omega_c s}{s^2 + 2\omega_c s + (h\omega)^2} \tag{17}$$

where h is the harmonic order, and k_{rh} is the resonant gain for each harmonic frequency. The open-loop Bode plots of compensated system by the PR controller with the 3rd to 7th harmonic compensators is shown in Fig. 6. The 3rd, 5th, and 7th harmonics are the most prominent harmonics under the grid environment. Like the PR controller, HC provides the high gain at selected harmonic frequency components, which helps eliminating steady-state error and the disturbance by the selected frequency components. Compared to the compensated system by the conventional PI controller shown in Fig. 5, it is obvious that the PR controller with harmonic compensators brings the higher gain at the fundamental and its harmonic frequencies of the grid without high proportional gain. In addition, the bandwidth in DCM is increased. Thus, it enhances the reference tracking speed and disturbance rejection performances with satisfaction of the desired stability in both operation modes.

The overall proposed control system for the flyback inverter with hybrid mode is shown in Fig. 7; it consists of the PR controller with HC and the nominal duty ratio D_n. I_g^* is the peak value of the reference grid current (or output current). As a kind

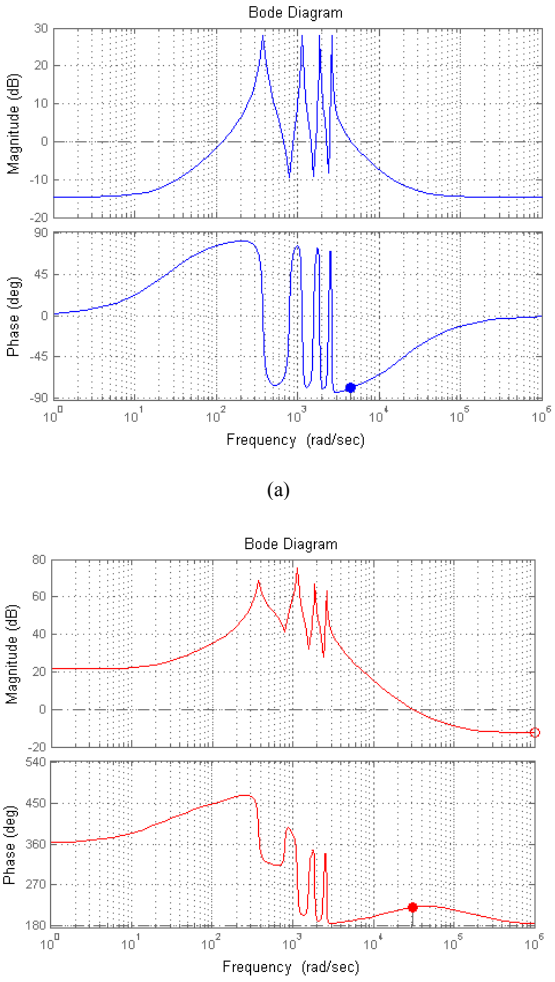

Fig. 6. Open-loop Bode plots of the compensated system by the proposed controller. (a) In DCM. (b) In CCM.

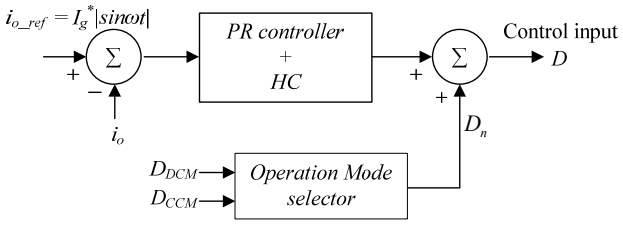

Fig. 7. The block diagram of the proposed control system.

of the feedforward control inputs, the nominal duty ratio D_n eliminates the disturbance effects and reduces the burden of the feedback controller. In [17], only the duty ratio D_{ccm} in (6) is applied to whole ac line period. In this case, the duty ratio D_{ccm} causes the voltage mismatch in the DCM region, which increases the burden of the feedback controller. Since the system gain in DCM is relatively lower, this burden becomes heavier. To overcome the mismatch in DCM, the duty ratio D_{DCM} should

This article has been accepted for publication in a future issue of this journal, but has not been fully edited. Content may change prior to final publication. Citation information: DOI 10.1109/TIE.2015.2481365, IEEE Transactions on Industrial Electronics

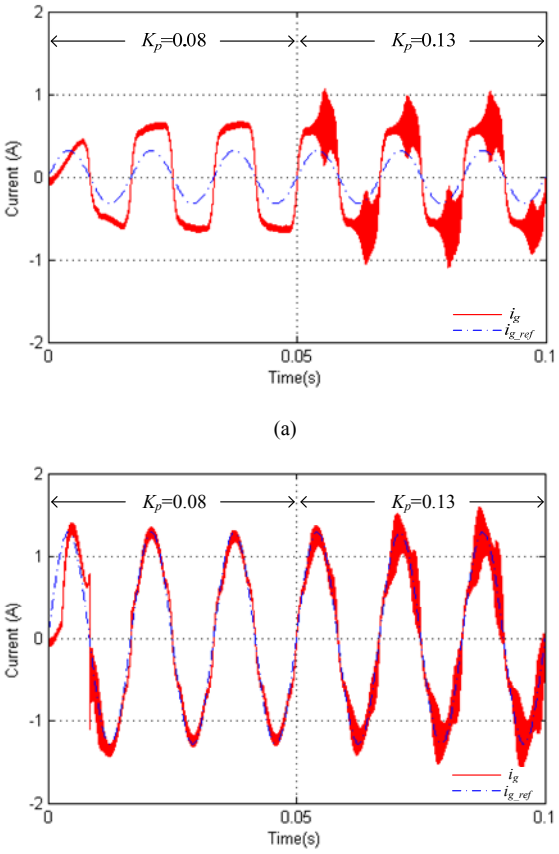

Fig. 8. Simulation results for the grid current i_g and its reference i_{g_ref} when the conventional control system is applied. (a) quarter-load condition. (b) full-load condition.

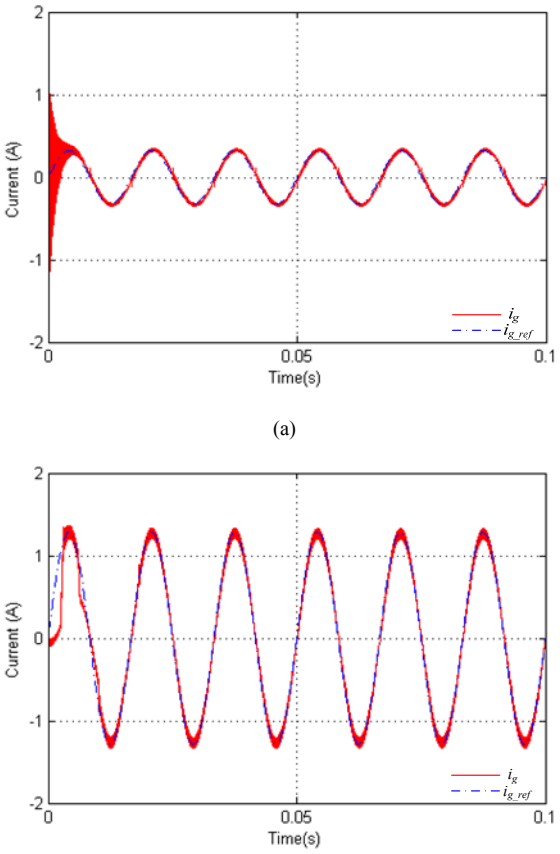

Fig. 9. Simulation results for the grid current i_g and its reference i_{g_ref} when the proposed control system is applied. (a) quarter-load condition. (b) full-load condition.

be applied when the flyback inverter operates in the DCM region; it means that the nominal duty ratio should be determined according to the operation region. To classify the section of operation modes without an additional current sensor, the critical duty ratio in (11) can be used; it is noted that the flyback inverter operates in the DCM region when the following condition is satisfied as

$$D_{DCM}(t) \le D_{CCM}(t). \tag{18}$$

Thus, the hybrid nominal duty ratio D_n in the proposed control strategy is determined as follows:

$$D_n(t) = \begin{cases} D_{DCM}(t), & \text{if } D_{DCM}(t) \le D_{CCM}(t) \\ D_{CCM}(t), & \text{if } D_{DCM}(t) > D_{CCM}(t) \end{cases}. \tag{19}$$

Finally, the proposed hybrid nominal duty ratio can significantly reduce the disturbance effect in both operation modes, and so improve the performance of the feedback controller.

TABLE I
PARAMETERS AND COMPONENTS OF THE PROTOTYPE

Parameters	**Symbols**	**Value**
PV voltage	V_{PV}	40-80V
Grid voltage	v_g	210V_{rms}
Grid frequency	f	60Hz
Rated average output power	P_o	200W
Switching frequency	f_s	60kHz
Primary winding turns	N_p	14turns
Secondary winding turns	N_s	51turns
Magnetizing inductance	L_m	50μH
Leakage inductance	L_{lk}	0.6μH
Input capacitor	C_{in}	6.6mF
Output capacitor	C_o	0.68μF
Output inductor	L_o	400μH
Components	*Symbols*	
Main switch	S_1	IPP200N25N3G
Unfold-bridge switches	S_2, S_3, S_4, S_5	IPP60R074C6
Rectifier diode	D_1	C2D05120A

This article has been accepted for publication in a future issue of this journal, but has not been fully edited. Content may change prior to final publication. Citation information: DOI 10.1109/TIE.2015.2481365, IEEE Transactions on Industrial Electronics

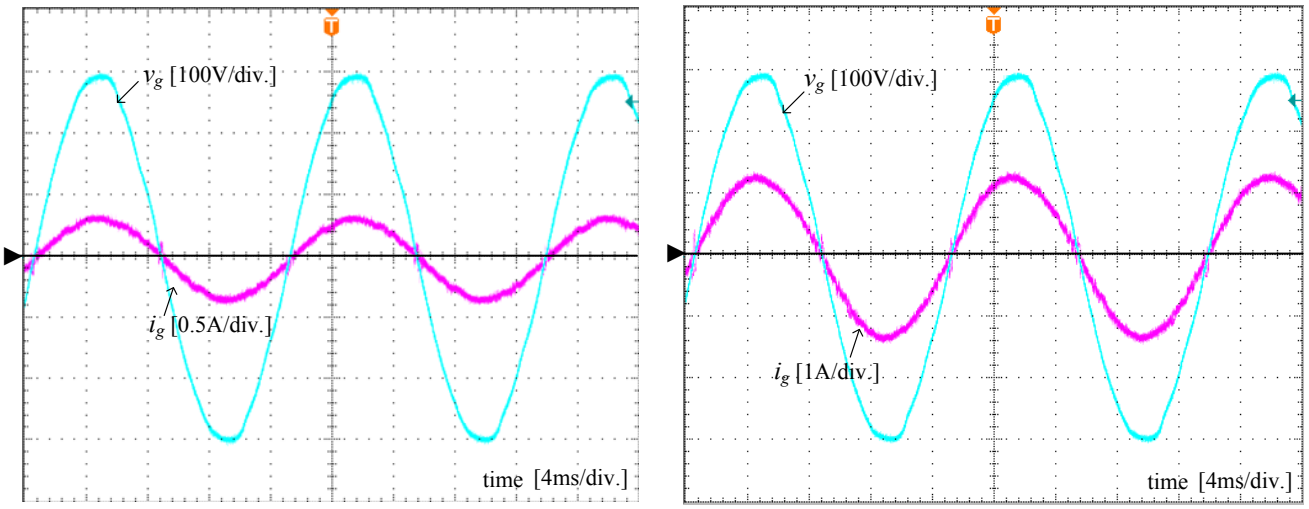

Fig. 10. Experimental results for grid voltage v_g and grid current i_g using the proposed control strategy. (a) quarter-load condition (only DCM region). (b) full-load condition (boundary between DCM and CCM regions, v_g=150V).

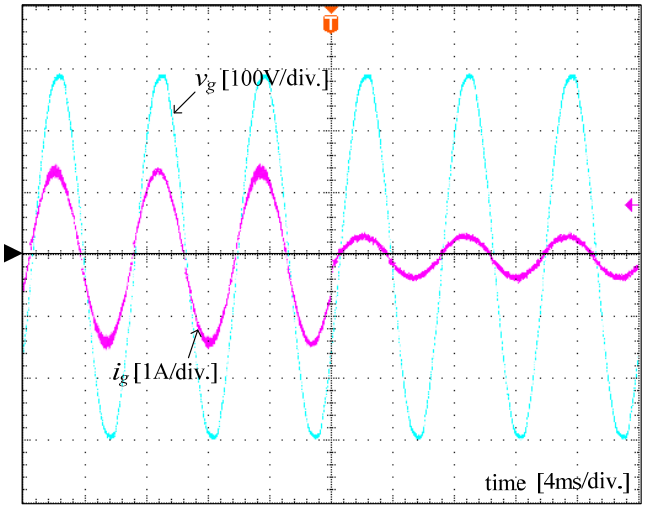

Fig. 11. Experimental result on the transient response under load variation from full-load to quarter-load.

IV. Simulation and Experimental Results

To verify the feasibility and performance of the proposed control strategy, the simulation by a simulator Psim and experiment using the prototype for the flyback microinverter shown in Fig. 1 were conducted. The nominal PV voltage and rated power were set up to 60V and 200W, respectively. The detail system parameters and parts are listed in Table I. Based on the analysis in the Section III, the controller parameters are designed. The prototype was implemented using Microchip, dsPIC33EP512GM604 under 25 kHz sampling frequency.

Fig. 8 shows the output current control performance when the conventional PI controller only with the duty ratio D_{CCM} in (6) is used. When the conventional control system is used, the grid current is distorted in the low power level. If the gain k_p increases to track the reference signal, the system becomes unstable. Especially, the output current is not regulated by the poor tracking and rejecting disturbance performances in the power level only with DCM region over whole ac line period. On the other hand, in the proposed control strategy, it is observed that the output current tracks the reference current and achieves the almost zero tracking error without high proportional gain as shown in Fig. 9.

Fig. 10 shows the experimental waveforms for the grid voltage and current when the proposed control strategy is applied. As shown in Fig. 10, regardless of load conditions, the grid current has an almost perfect sinusoidal form and desired power level. The THD on the grid current is measured as 2.4% under full-load condition. Fig. 11 shows the dynamic performance under the load variation. From Fig.11, it is verified that the proposed control system makes output current well track its desired value under the load transient-state.

Fig. 12 shows the current stress between the flyback inverter with hybrid mode and the flyback inverter operating only in DCM region. To ensure DCM operation for all operating points, the magnetizing inductance of the DCM flyback is set to 11uH. From Fig. 12, it is observed that the flyback with hybrid mode has much lower current stress in both primary and secondary sides than those of the DCM flyback inverter. Fig. 13 represents efficiency comparison for the two flyback inverters according to load conditions; it is obvious that the flyback inverter with hybrid mode has higher efficiency over all load conditions. Its maximum efficiency is measured to be 96.1%.

V. Conclusion

The current control strategy of the flyback microinverter with hybrid mode for PV ac module has been introduced and verified by the analysis, simulation, and experimental results. In the proposed control strategy, the PR controller with HC provides the high system gain at fundamental and harmonic

This article has been accepted for publication in a future issue of this journal, but has not been fully edited. Content may change prior to final publication. Citation information: DOI 10.1109/TIE.2015.2481365, IEEE Transactions on Industrial Electronics

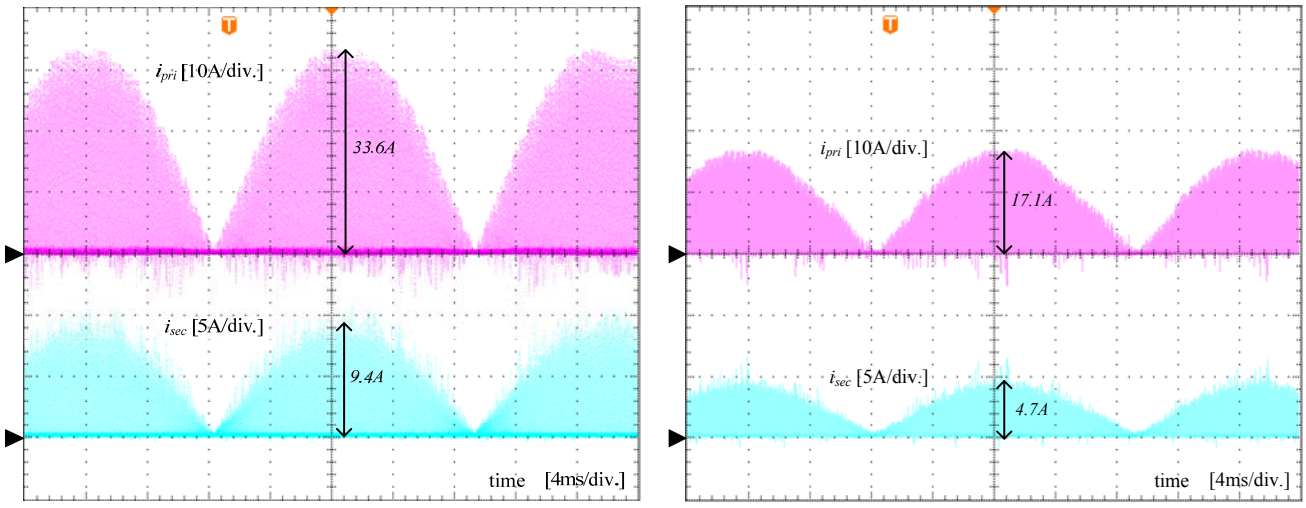

(a) (b)

Fig. 12. Comparison for current stress under full-load condition. (a) In a DCM flyback inverter. (b) In a flyback inverter with hybrid mode.

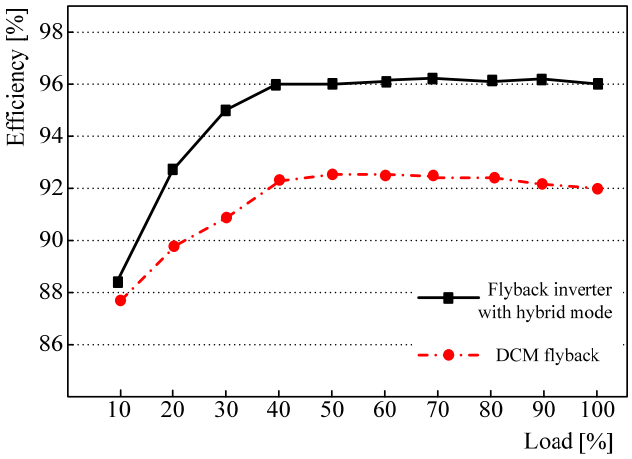

Fig. 13. Efficiency comparison according to load conditions.

frequencies in both operation modes without using high proportional gain. The characteristic alleviates the trade-off between the control performance in DCM and stability in CCM when the conventional PI controller is used. In addition, the proposed hybrid nominal duty ratio yielded from the proposed operation mode selection eliminates the disturbance more effectively and reduces the burden of the feedback controller. From the simulation and experiment results, it is verified that the proposed control strategy shows faster reference tracking and better disturbance rejection than those of the conventional strategy. Finally, the proposed control strategy encourages the many advantages of the flyback inverter with hybrid mode and makes it to be used in the industrial field.

REFERENCES

[1] Y. –H. Kim, J. –W. Jang, S. –C. Shin, and C. –Y. Won, " Weighted-efficiency enhancement control for a photovoltaic AC module interleaved flyback inverter using a synchronous rectifier," *IEEE Trans. Power Electron.*, vol. 29, no .12, pp. 6481–6493. Dec. 2014.

[2] G. Petrone, G. Spagnuolo, and M. Vitelli, "An analog technique for distributed MPPT PV applications," *IEEE Trans. Ind. Electron.*, vol. 59, no. 12, pp. 4713-4722, Dec. 2012.

[3] H. –J. Chiu, Y. –K. Lo, C. –Y. Yang, S. –J. Cheng, C. –M. Huang, C. –C. Chuang, M. –C. Kuo, Y. –M. Huang, Y. –B. Jean, and Y. –C. Huang, "A module- integrated isolated solar microinverter," *IEEE Trans. Ind. Electron.*, vol. 60, no. 2, pp. 781-788, Feb. 2013.

[4] N. Sukesh, M. Pahlevaninezhad, and P. K. Jain, "Analysis and implementation of a single-stage flyback PV microinverter with soft switching," *IEEE Trans. Ind. Electron.*, vol. 61, no .4, pp. 1819–1833. Dec. 2014.

[5] M. Gao, M. Chen, C. Zhang, and Z. Qian, "Analysis and implementation of an improved flyback inverter for photovoltaic ac module applications," *IEEE Trans. Power. Electron.*, vol. 29, no .7, pp. 3428–3444. Jul. 2014.

[6] A. C. Nanakos, E. C. Tatakis, and N. P. Papanikolaou, "A weighted-efficiency-oriented design methology of flyback inverter for ac photovoltaic modules," *IEEE Trans. Power. Electron.*, vol. 27, no .7, pp. 3221–3233. Jul. 2012.

[7] T. Shimizu, K. Wada, and N. Nakamura, "A flyback-type single phase utility interactive inverter with low-frequency ripple current reduction on the dc input for an ac photovoltaic module system," in *Proc. Power Electron. Spec. Conf.* (*PESC*), 2002, pp. 1483–1488.

[8] W. J. Cha, C. Y. Cho, J. M. Kwon, and B. H. Kwon, "Highly-efficient microinverter with soft-switching step-up converter and single-switch-modulation inverter," *IEEE Trans. Ind. Electron.*, vol. 62, no. 6, pp. 3516-3523. Jun. 2015.

[9] Z. Zhang, X. –F. He, and Y. –F. Liu, "An optimal control method for photovoltaic grid-tied-interleaved flyback microinverters to achieve high efficiency in wide load range," *IEEE Trans. Power. Electron.*, vol. 28, no .11, pp. 5074–5087. Nov. 2013.

[10] Y. –H. Kim, Y. –H. Ji, J. –G. Kim, Y. –C. Jung, and C. –Y. Won, "A new control strategy for improving weighted efficiency in photovoltaic ac module-type interleaved flyback inverter," *IEEE Trans. Power. Electron.*, vol. 28, no .6, pp. 2688–2699. Jun. 2013.

[11] A. C. Kyritsis, E. C. Tatakis, and N. P. Papanikolaou, "Optimum design of the current-source flyback inverter for decentralized grid-connected photovoltaic systems," *IEEE Trans. Energy. Convers.*, vol. 23, no .1, pp. 281–293. Mar. 2008.

[12] H. Hu, S. Harb, N. H. Kutkut, Z. J. Shen, and I. Batarseh, "A single-stage microinverter without using electrolytic capacitors," *IEEE Trans. Power. Electron.*, vol. 28, no .6, pp. 2677–2687. Jun. 2013.

[13] S. Zengin, F. Deveci, and M. Boztepe, "Decoupling capacitor selection in DCM flyback PV microinverters considering harmonic distortion," *IEEE Trans. Power. Electron.*, vol. 28, no .2, pp. 816–825. Feb. 2013.

[14] Y. –C. Hsieh, M. –R. Chen, and H. –L. Cheng, "Zero-voltage-switched interleaved flyback converter," in *Proc. 31st INTELEC*, 2009, pp. 1-6.

This article has been accepted for publication in a future issue of this journal, but has not been fully edited. Content may change prior to final publication. Citation information: DOI 10.1109/TIE.2015.2481365, IEEE Transactions on Industrial Electronics

[15] Y. Li and R. Oruganti, "A low cost flyback CCM inverter for AC module application," *IEEE Trans*. *Power Electron*., vol. 27, no. 3, pp. 1295-1303, Mar. 2012.
[16] T. V. Thang, N. M. Thao, D. –H. Kim, and J. –H. Park, "Analysis and design of grid-connected photovoltaic systems with multiple-integrated converters and a pseudo-dc-link inverter," *IEEE Trans*. *Ind*. *Electron*., vol. 61, no. 7, pp. 3377-3386, Jul. 2014.
[17] F. F. Edwin, W. Xiao, and V. Khadkikar, "Dynamic modeling and control of interleaved flyback module-integrated converter for PV power applications," *IEEE Trans*. *Ind*. *Electron*., vol. 61, no. 3, pp. 1377-1388, Mar. 2014.
[18] G. Shen, X. Zhu, J. Zhang, and D. Xu, "A new feedback method for PR current control of LCL-filter-based grid-connected inverter," *IEEE Trans*. *Ind*. *Electron*., vol. 57, no. 6, pp. 2033-2041, Jun. 2010.
[19] S. –Y. Park, C. –L. Chen, J. –S. Lai, and S. –R. Moon, "Admittance Compensation in Current Loop Control Proportional-resonant controllers for grid-tie LCL fuel cell inverter," *IEEE Trans*. *Power Electron*., vol. 23, no. 4, pp. 1716-1723, Jul. 2008.
[20] R. Teodorescu, F. Blaabjerg, M. Liserre, and P. C. Loh, "Proportional-resonant controllers and filters for grid-connected voltage-source converters," *IEE Proc. Electron. Power Appl.*, vol. 153, no. 5, pp. 750-762, Sep. 2006.

Sung-Ho Lee was born in Seoul, Korea, in 1985. He received the B.S degree in electrical engineering from Dongguk University, Seoul, Korea, in 2011. He is currently working toward the Ph.D. degree in electronic and electrical engineering in Pohang University of Science and Technology, (POSTECH), Pohang, Korea. His research interests include dc-dc converters, grid-connected inverters, and renewable energy system.

Woo-Jun Cha was born in Inchon, Korea, in 1979. He received the M.S. degree in electronic systems engineering from Hanyang University, Ansan, Korea, in 2013. He is currently working toward the Ph.D. degree in electronic and electrical engineering at the Pohang university of Science and Technology (POSTECH), Pohang, Korea. His main research interests include photovoltaic systems, switched-mode power supplies, and advanced LED lighting solutions.

Jung-Min Kwon (M'09) was born in Ulsan, Korea, in 1981. He received the B.S. degree in electrical and electronic engineering from Yonsei University, Seoul, Korea, in 2004, and the Ph.D. degree in electronic and electrical engineering from Pohang University of Science and Technology (POSTECH), Pohang, Korea, in 2009.

From 2009 to 2011, he has been with the Samsung Advanced Institute of Technology, Yongin, Korea. Since 2011, he has been with the Department of Electrical Engineering, Hanbat National University, Daejeon, Korea, where he is currently a Professor. His research interests include direct methanol fuel cell, renewable energy system, and distributed generation.

Bong-Hwan Kwon (M'91) was born in Pohang, Korea, in 1958. He received the B.S. degree from the Kyungpook National University, Deagu, Korea, in 1982 and the M.S. and Ph.D. degrees in electrical engineering from the Korea Advanced Institute of Science and Technology, Seoul, Korea, in 1984 and 1987, respectively.

Since 1987, he has been with the Department of Electronic and Electrical Engineering, Pohang University of Science and Technology (POSTECH), Pohang, Korea, where he is currently a Professor. His research interests include converters for renewable energy, high-frequency converters, and switch-mode power supplies.